sealed under vacuum (<0.015 torr). The other three reaction solutions shown in Table II were prepared in a similar fashion. Solutions were decomposed thermally in a constant temperature oil bath at 133 ± 0.5 °C with no stirring. The extent of decomposition was determined by comparing the integrals of the ^{31}P NMR resonances of L^D_2PtDCl and starting material. The kinetics at decomposition were half-order in $L^D_2PtNp^DCl$.[55] Solutions were thermally decomposed for 15 h or until ~25% of $L^D_2PtNp^DCl$ remained. After the volatiles were condensed by cooling with liquid nitrogen, tubes were opened and sealed with a septum. The liquid phase of each tube was analyzed by GC and GC/MS. The relative amounts of neopentane-d_{11} and neopentane-d_{12} were determined by comparing the relative abundance of the m/e 65 and 66 peaks of the product neopentane with the m/e peaks of authentic samples of neopentane-d_{11} (65/100%, 66/39%) and neopentane-d_{12} (65/11.4, 66/100%).[80,85]

Supplementary Material Available: Synthesis and characterization of triethylphosphine-d_{15} and several 3,3,4,4-tetramethylmetallacyclopentanes (bis(tri-*n*-butylphosphine)-3,3,4,4-tetramethylplatinacyclopentane; bis(triethylphosphine)-3,3,4,4-tetramethylplatinacyclopentane; 1-phenyl-3,3,4,4-tetramethylphospholane oxide; 1-phenyl-3,3,4,4-tetramethylphospholane; 1,1-diphenyl-3,3,4,4-tetramethylsilacyclopentane; 1,1,3,3,4,4-hexamethylsilacyclopentane; 1,1-diphenyl-3,3,4,4-tetramethylstannacyclopentane; and 1,1-diphenyl-3,3,4,4-tetramethylgermacyclopentane) (11 pages). Ordering information is given on any current masthead page.

Reactivity and Conformation of a Phosphine-Substituted Dihalocarbene Complex. X-ray Crystal Structures of $[(\eta^5\text{-}C_5H_5)Fe(CO)(PPh_3)(CF_2)][BF_4]$ and $[(\eta^5\text{-}C_5H_5)Fe(CO)_2(CCl_2)][BCl_4]$

Ann M. Crespi and Duward F. Shriver*

Department of Chemistry, Northwestern University, Evanston, Illinois 60201

Received March 12, 1985

The difluorocarbene complex $[CpFe(CO)(PPh_3)(CF_2)][BF_4]$ (1) was prepared by halide abstraction from $CpFe(CO)(PPh_3)(CF_3)$ using BF_3. The structures of this compound and $[CpFe(CO)_2(CCl_2)][BCl_4]$, **2**, determined by single-crystal X-ray diffraction, show the effect of ligand asymmetry on the dihalocarbene orientation. For **1** the plane of the CF_2 ligand is tilted 18° away from coplanarity with the CO. Complex **2** adopts a vertical conformation with the plane of the CCl_2 ligand bisecting the OC–Fe–CO angle. The orientations of CX_2 in **1** and **2** agree with the conformations predicted by the MO treatment of Hoffmann and co-workers; however, low-temperature NMR measurements of **1** indicate that the CF_2 group is rapidly rotating in solution, so the energy barrier between the various conformers is low. The reaction of $CpFe(CO)(PPh_3)(CF_3)$ with BCl_3 at low temperatures was followed by low temperature NMR, which indicates the successive formation of CF_2, CFCl, and CCl_2 complexes. These results substantiate a previously postulated mechanism for halide exchange. Crystal data for **1**: space group, monoclinic, $P2_1/c$; a = 9.035 (3) Å, b = 24.390 (11) Å, c = 10.745 (5) Å, β = 102.20 (3)°; Z = 4. Crystal data for **2**: space group, monoclinic, $P2_1/c$; a = 12.238 (4) Å, b = 9.444 (4) Å, c = 13.440 (4) Å, β = 113.55 (3)°; Z = 4.

Introduction

Dihalocarbene transition-metal complexes are versatile precursors to other ligands.[1-8] For example, dihalocarbenes react with nucleophiles to form substituted carbenes as well as nitriles, isonitriles, and thiocarbonyls[2,4-6,8] (eq 1–3). An unusual difluorocarbene of Ru(0), $[Ru(CF_2)(CO)_2(PPh_3)_2]$, also reacts with electrophiles.[7] One convenient method of synthesizing cationic dihalocarbene complexes and neutral trihalomethyl complexes is halogen exchange and halide abstraction of trifluoromethyl complexes using boron trihalides (eq 4–6).[1,2]

$$IrCl_2(CCl_2)(PPh_3)_2 + H_2S \rightarrow IrCl_2(CS)(PPh_3)_2 + 2HCl \quad (1)$$

$$RuCl_2(CCl_2)(CO)(PPh_3)_2 + H_2NCH_3 \rightarrow RuCl_2(CNCH_3)(CO)(PPh_3)_2 + 2HCl \quad (2)$$

$$RuCl_2(CCl_2)(CO)(PPh_3)_2 + HSCH_2CH_2SH \rightarrow RuCl_2(CSCH_2CH_2S)(CO)(PPh_3)_2 + 2HCl \quad (3)$$

$$CpFe(CO)_2(CF_3) + 2BCl_3 \rightarrow [CpFe(CO)_2(CCl_2)][BCl_4] + BF_3 \quad (4)$$

$$CpFe(CO)_2(CF_3) + BF_3 \rightarrow [CpFe(CO)_2(CF_2)][BF_4] \quad (5)$$

$$CpFe(CO)_2(CF_3) + BCl_3 \rightarrow CpFe(CO)_2(CCl_3) + BF_3 \quad (6)$$

In the proposed mechanism for the reaction in eq 6 halogen exchange proceeds through dihalocarbene intermediates. However, a concerted mechanism could not be ruled out.[1] Ligand substitution of carbene complexes alters both the reactivity and geometric conformation of the complex. The carbene ligand behaves as a π-acid. Since PPh_3 donates more electron density to the metal center than does CO, one would expect phosphine substitution to facilitate halide abstraction and stabilize the carbene. In this paper a comparison of the reactivities of $CpFe(CO)(PPh_3)(CF_3)$ and $CpFe(CO)_2(CF_3)$ with BCl_3 demonstrates this stabilization of the carbene and provides evidence for the carbene exchange mechanism.

(1) Richmond, T. G.; Shriver, D. F. *Organometallics* **1984**, *3*, 305–314.
(2) Richmond, T. G.; Crespi, A. M.; Shriver, D. F. *Organometallics* **1984**, *3*, 314–319.
(3) Reger, D. L.; Dukes, M. D. *J. Organomet. Chem.* **1978**, *153*, 67–72.
(4) Clark, G. R.; Marsden, K.; Roper, W. R.; Wright, L. J. *J. Am. Chem. Soc.* **1980**, *102*, 1206–1207.
(5) Clark, G. R.; Hoskins, S. V.; Roper, W. R. *J. Organomet. Chem.* **1982**, *234*, C9–C12.
(6) Clark, G. R.; Roper, W. R.; Wright, A. H. *J. Organomet. Chem.* **1982**, *236*, C7–C10.
(7) Clark, G. R.; Hoskins, S. V.; Jones, J. C.; Roper, W. R. *J. Chem. Soc., Chem. Commun.* **1983**, 719–721.
(8) Roper, W. R.; Wright, A. H. *J. Organomet. Chem.* **1982**, *233*, C59–C63.

0276-7333/85/2304-1830$01.50/0

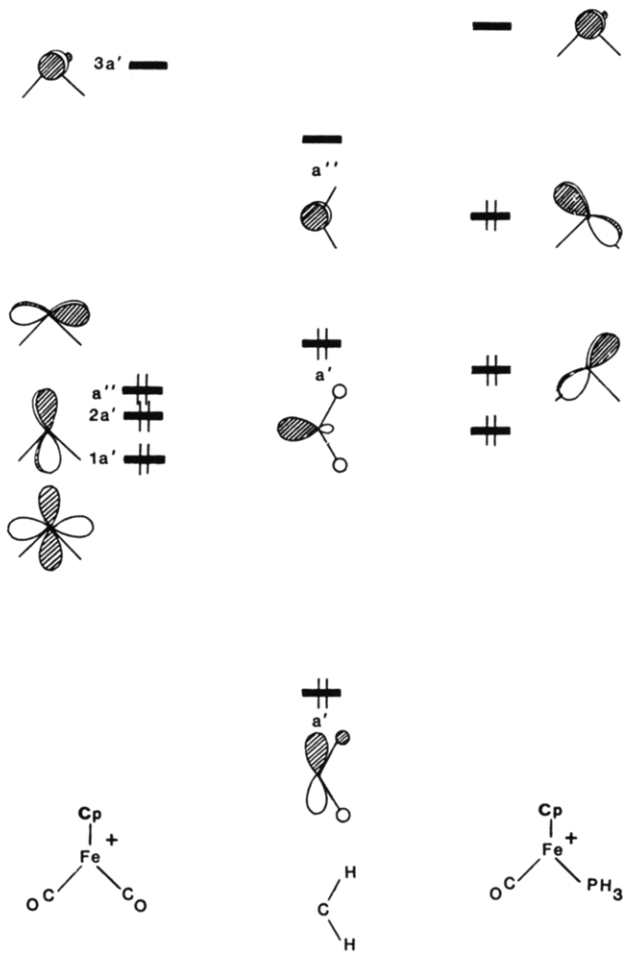

Figure 1. The valence orbitals for the fragments $CpFe(CO)_2^+$, CH_2, and $CpFe(CO)(PH_3)^+$.

Theoretical calculations predict that for the carbene complexes of the type $CpM(CO)(L)(CH_2)$ (L = CO, NO^+, PPh_3),[9-11] the symmetrical complex (L = CO) will lead the carbene to lie in a plane which bisects the CO–M–CO angle. The carbene moiety in an unsymmetrically substituted complex (L = NO^+, PPh_3) is predicted to be coplanar with the better π-acceptor. Substitution of CO by PH_3 splits the near degeneracy of the a'' and 2a' orbitals on the $CpFe(CO)(PH_3)^+$ fragment and reorients the orbitals, as shown in Figure 1.[9,10] The LUMO of the carbene, the a'' orbital, interacts with the HOMO's of the metal fragments. Thus, compounds **1** and **2** are predicted to adopt the conformations below. X-ray crystal structure

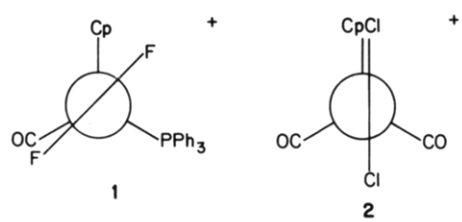

determinations of complexes of **1** and **2** were undertaken to determine whether the orientation of the carbenes agrees with the theoretical predictions. The structural information is discussed with respect to electronic and steric effects in these complexes.

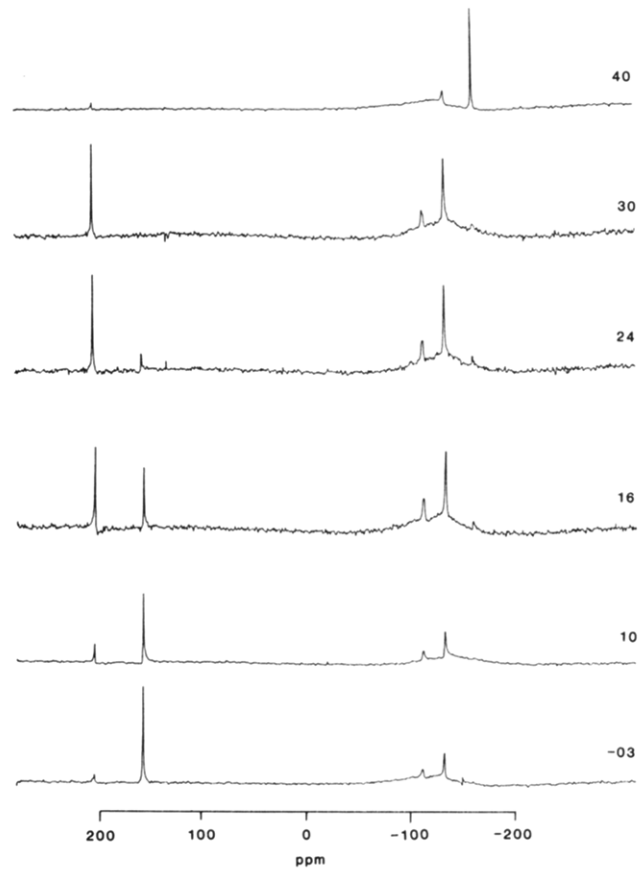

Figure 2. Variable-temperature 84.25-MHz ^{19}F NMR spectra of $CpFe(CO)(PPh_3)(CF_3)$ + BCl_3 in CD_2Cl_2 (reference external $CFCl_3$).

Experimental Section

General Data. All manipulations were carried out by using standard Schlenk and syringe techniques,[12] a high-vacuum manifold fitted with grease-free Teflon-in-glass valves, and a Vacuum Atmospheres glovebox. Solvents were freed of oxygen and dried immediately prior to use. For manipulations involving **1**, the glassware was treated with Glassclad 6C, a silylating agent supplied by Petrarch Inc., and dried in a 110 °C oven to remove surface moisture.

The compounds $CpFe(CO)(PPh_3)(CF_3)$ and $[CpFe(CO)_2(CCl_2)][BCl_4]$ were prepared as described in the literature and identified by IR and ^1H NMR spectroscopy.[2,13] Fractionation through two traps held at −78 °C was performed to purify BF_3, and BCl_3 was degassed at −78 °C to remove HCl.

Instrumentation. IR spectra were recorded on a Perkin-Elmer 283 spectrometer, for samples in Nujol mulls using KBr plates or in solution using 0.1-mm cells with CaF_2 windows. A JEOL FX-90 spectrometer with a variable-temperature accessory was used to record ^1H and ^{19}F NMR spectra, and ^{13}C NMR spectra were recorded on a JEOL FX-270 spectrometer. The reference for ^1H and ^{13}C spectra was external Me_4Si, and ^{19}F spectra were referenced against external $CFCl_3$, taking a downfield shift as positive.

Preparation of $[CpFe(CO)(PPh_3)(CF_2)][BF_4]$. A solution of 85 mg (0.18 mmol) of $CpFe(CO)(PPh_3)(CF_3)$ in 3 mL of CH_2Cl_2 was treated with 0.36 mmol of BF_3. Slow evaporation of solvent afforded yellow crystals of product in a yield of 40 mg (11%). The product is extremely moisture sensitive in solution and solid state, forming $CpFe(CO)_2(PPh_3)^+$ as the hydrolysis product. Owing to this extreme moisture sensitivity, the product was usually gen-

(9) Schilling, B. E. R.; Hoffmann, R.; Lichtenberger, D. L. *J. Am. Chem. Soc.* **1979**, *101*, 585–591.
(10) Schilling, B. E. R.; Hoffmann, R.; Faller, J. W. *J. Am. Chem. Soc.* **1979**, *101*, 592–598.
(11) Kostic, N. M.; Fenske, R. F. *J. Am. Chem. Soc.* **1982**, *104*, 3879–3884.
(12) Shriver, D. F. "Manipulation of Air Sensitive Compounds"; McGraw Hill: New York, 1969.
(13) King, R. B.; Kapoor, R. N.; Parnell, K. H. *J. Organomet. Chem.* **1969**, *20*, 187–193.

Table I. Crystallographic Data

	1	2
formula	$C_{25}H_{20}BF_6FeOP$	$C_8H_5BCl_6FeO_2$
mol wt	548.06	412.50
space group	$P2_1/c$	$p2_1/c$
a, Å	9.035 (3)	12.238 (4)
b, Å	24.390 (11)	9.444 (4)
c, Å	10.745 (5)	13.440 (4)
β, deg	102.20 (3)	113.55 (3)
vol, Å^3	2314.27	1423.96
Z	4	4
d_{calcd}, g cm^{-1}	1.573	1.924
abs coeff (μ), cm^{-1}	7.8	21.8
crystal	hex plate, 0.32 × 0.28 × 0.09	prism, 0.3 × 0.2 × 0.2
scan speed, deg min^{-1}	2.7	5.3
scan range, 2θ, deg	3–50	3–50
scan mode	–2	–2
reflctns measd	$h,k,\pm l$	$h,k,\pm l$
stds	(–5,8,5)(–1,–2,5)(–2,0,4)	(1,1,0)(2,–1,3)(0,–1,4)
	(0,–1,5)(0,8,0)(–1,0,8)	(1,4,0)(0,0,10)
	every 12 000	every 6000 s
decay of stds	none	–23%
unique data	4058	2485
data, $I > 3\ \sigma(I)$	1514	1298
temp of data collection, K	233K	133K

erated in solution and used immediately without isolation: IR (Nujol mull) ν_{CO} 2024 (s), ν_{CF} 1198 (s), 1182 (sh) cm^{-1}; ^{13}C NMR (CD_2Cl_2) δ 216 (CO), 139 (Ph), 95 (Cp) (the ^{13}C signal for the carbene was not observed presumably because it is split by F and P); ^{19}F NMR (CD_2Cl_2) δ 164 (s, CF_2), –149 (s, BF_4^-); ^{1}H NMR (CD_2Cl_2) δ 7.56 (m, Ph), 5.30 (s, Cp). Calcd for $C_{25}H_{20}BF_6FeOP$: C, 54.74; H, 3.65; B, 1.97; F, 20.81; P, 5.66. Found: C, 50.72; H, 3.46; B, 1.88; F, 15.05; P, 5.56.

CpFe(CO)(PPh$_3$)(CF$_3$) + BCl$_3$. A solution of 28 mg (0.058 mmol) of CpFe(CO)(PPh$_3$)(CF$_3$) in 2 mL of CD_2Cl_2 was treated with 0.058 mmol of BCl_3. The sample was maintained at –78 °C until it was slowly warmed and monitored by ^{19}F NMR, as summarized in Figure 2. The solution IR (CD_2Cl_2) of the sample showed one band at ν_{CO} 2030 cm^{-1}.

X-ray Data Collection and Refinement of Structure. Orange crystals of [CpFe(CO)$_2$(CCl$_2$)][BCl$_4$] were grown by slow cooling of a solution of CH_2Cl_2. Crystals of [CpFe(CO)(PPh$_3$)(CF$_2$)][BF$_4$] were grown as yellow plates by slow evaporation of CH_2Cl_2. Both crystals were mounted in capillaries in a nitrogen-filled glovebag and sealed under N_2. Least-squares refinement of 25 centered reflections produced the final unit cell parameters. Data were collected on an Enraf-Nonius CAD-4 diffractometer, using Mo Kα radiation with a graphite monochromator. Crystallographic data and the data collection parameters are summarized in Table I.

Calculations were carried out by using the Enraf-Nonius SDP-Plus crystallographic computing package. In each case, the iron atom was located by a Patterson map and the other nonhydrogen atoms were located by Fourier techniques. The structures were refined by using full-matrix least-squares techniques based on minimizing $\sum w(|F_o| - |F_c|)^2$, where $w = 4F_o^2/[\sigma^2(F_o)^2 + (pF_o^2)^2]$ and $p = 0.05$. Hydrogen atoms were added in idealized positions and included in structure factor calculations but were not refined. Scattering factors and corrections for anomalous dispersion were taken from ref 14. An absorption correction was applied to 2, using the empirical psi-scan technique. The minimum and maximum correction factors were 0.7373 and 0.9992, respectively. All non-hydrogen atoms were refined anisotropically, with the exception of C(1), C(4), C(6), and C(7). These atoms showed nonpositive definite anisotropic thermal parameters, so they were refined isotropically. The thermal instability of this complex resulted in a 23% loss of intensity of the standard reflections during data collection. In separate experiments it was found that **2** decomposes according to eq 7 and 8.[1,2] Data were corrected for loss of intensity using the program CHORT in SDP-Plus. Least-squares refinement converged with residuals of $R = 8.4$, $R_w = 10.9$. The unweighted R factor including unobserved reflections was $R = 15.5$, indicating reasonable agreement between observed and calculated structure amplitudes for this large number of weak reflections. Decomposition of the

$$[CpFe(CO)_2(CCl_2)][BCl_4] \rightarrow CpFe(CO)_2(CCl_3) + BCl_3 \quad (7)$$

$$CpFe(CO)_2(CCl_3) \rightarrow HCl + \ldots \quad (8)$$

(14) "International Tables for X-ray Crystallography"; The Kynoch Press: Birmingham, England, 1974; Vol. IV.

Table II. Fractional Coordinates of Non-Hydrogen Atoms for [CpFe(CO)(PPh$_3$)(CF$_2$)][BF$_4$][a]

atom	x	y	z
Fe	0.6816 (1)	0.42663 (5)	0.2679 (1)
P	0.8314 (2)	0.35239 (9)	0.2913 (2)
F(1)	0.5222 (6)	0.4033 (2)	0.4563 (5)
F(2)	0.4448 (6)	0.3580 (2)	0.2987 (6)
F(3)	0.3052 (7)	0.4949 (3)	0.1027 (6)
F(4)	0.2510 (8)	0.4718 (3)	0.2866 (6)
F(5)	0.0931 (7)	0.5253 (3)	0.1544 (7)
F(6)	0.3194 (8)	0.5565 (3)	0.2567 (8)
O	0.5150 (8)	0.4007 (3)	0.0121 (6)
C(1)	0.5519 (9)	0.3951 (4)	0.3412 (8)
C(2)	0.5791 (9)	0.4095 (3)	0.1104 (8)
C(3)	0.879 (1)	0.4757 (3)	0.3218 (8)
C(4)	0.792 (1)	0.4777 (4)	0.4171 (8)
C(5)	0.650 (1)	0.5000 (3)	0.3579 (8)
C(6)	0.6470 (9)	0.5104 (3)	0.2286 (9)
C(7)	0.791 (1)	0.4952 (3)	0.2064 (8)
C(8)	0.9599 (9)	0.3546 (3)	0.4474 (7)
C(9)	1.1132 (9)	0.3636 (3)	0.4579 (8)
C(10)	1.2050 (9)	0.3710 (3)	0.5778 (8)
C(11)	1.148 (1)	0.3682 (3)	0.6856 (8)
C(12)	0.992 (1)	0.3591 (4)	0.6751 (8)
C(13)	0.9002 (9)	0.3522 (3)	0.5561 (7)
C(14)	0.9574 (8)	0.3422 (3)	0.1814 (7)
C(15)	1.038 (1)	0.2927 (3)	0.1864 (8)
C(16)	1.139 (1)	0.2837 (4)	0.1103 (8)
C(17)	1.1699 (9)	0.3256 (4)	0.0342 (8)
C(18)	1.093 (1)	0.3746 (4)	0.0254 (9)
C(19)	0.9879 (9)	0.3822 (3)	0.1004 (8)
C(20)	0.7344 (8)	0.2872 (3)	0.2792 (8)
C(21)	0.7728 (9)	0.2457 (4)	0.3714 (8)
C(22)	0.704 (1)	0.1948 (3)	0.3547 (8)
C(23)	0.598 (1)	0.1838 (2)	0.2443 (8)
C(24)	0.558 (1)	0.2246 (4)	0.1540 (8)
C(25)	0.6267 (9)	0.2756 (3)	0.1719 (8)
B	0.239 (1)	0.5130 (5)	0.198 (1)

[a] Numbers in parentheses are estimated standard deviations in the least significant digits. See Figure 3 for numbering scheme.

Table III. Fractional Coordinates of Non-Hydrogen Atoms for [CpFe(CO)$_2$(CCl$_2$)][BCl$_4$][a]

atom	x	y	z
Fe	0.2165 (2)	0.1480 (3)	0.4008 (2)
Cl(1)	0.2015 (4)	0.4228 (6)	0.5277 (4)
Cl(2)	–0.0128 (3)	0.2985 (6)	0.3937 (3)
Cl(3)	0.6940 (4)	0.2467 (5)	0.8331 (3)
Cl(4)	0.6897 (4)	0.3312 (6)	0.6133 (3)
Cl(5)	0.5277 (4)	0.4757 (6)	0.7016 (3)
Cl(6)	0.7917 (4)	0.5297 (6)	0.8030 (4)
O(1)	0.077 (1)	–0.082 (1)	0.4389 (9)
O(2)	0.048 (1)	0.162 (1)	0.1736 (8)
C(1)	0.366 (1)	0.031 (2)	0.489 (1)
C(2)	0.381 (1)	0.164 (2)	0.532 (1)
C(3)	0.378 (1)	0.259 (2)	0.449 (1)
C(4)	0.362 (1)	0.178 (2)	0.357 (1)
C(5)	0.353 (1)	0.037 (2)	0.380 (1)
C(6)	0.130 (1)	0.009 (2)	0.426 (1)
C(7)	0.113 (1e	0.158 (2)	0.261 (1)
C(8)	0.141 (1)	0.288 (22)	0.439 (1)
B	0.675 (2)	0.397 (2)	0.736 (1)

[a] Numbers in parentheses are estimated standard deviations in the least significant digits. See Figure 4 for numbering scheme.

crystal and the necessarily high scan speed contributed to the high R factors and esd's.

The crystal faces of 1 were indexed and a numerical absorption correction applied to the data, with minimum and maximum correction factors of 0.8100 and 0.9348, respectively. All nonhydrogen atoms were refined anisotropically. Least-squares refinement converged with residuals of $R = 4.8$, $R_w = 5.3$, and $R = 19.2$ when unobserved reflections are included.

Results and Discussion

The proposed pathway for halogen exchange between trifluoromethyl transition-metal complexes and boron trihalides proceeds via intermediate carbene complexes (eq 9–11). Repetitions of this sequence lead to the formation

$$M{-}CF_3 + BX_3 \rightarrow [M{=}CF_2]^+[F{-}BX_3]^- \quad (9)$$

$$[M{=}CF_2]^+[F{-}BX_3]^- \rightarrow [M{=}CF_2]^+[X{-}BFX_2]^- \quad (10)$$

$$[M{=}CF_2]^+[X{-}BFX_2]^- \rightarrow M{-}CF_2X + BFX_2 \quad (11)$$

of M–CX_3 and BF_3. For example, $CpFe(CO)_2(CF_3)$ reacts with 1 equiv of BCl_3 to produce $CpFe(CO)_2(CCl_3)$. The reaction proceeds to completion even at low temperatures and is driven by the formation of the very stable BF_3 molecule.[1]

Reaction with BCl_3. Treatment of $CpFe(CO)(PPh_3)(CF_3)$ with 1 equiv of BCl_3 at low temperature results in halide abstraction affording $CpFe(CO)(PPh_3)(CF_2)^+$ (see Figure 2). Upon warming the sample a new peak appears at δ 207 (s), which is assigned to $CpFe(CO)(PPh_3)(CFCl)^+$. The intensity of the chlorofluorocarbene increases relative to the difluorocarbene as warming continues. At +40 °C the signal from $CpFe(CO)(PPh_3)(CFCl)^+$ nearly disappears, indicating that the favored species is $CpFe(CO)(PPh_3)(CCl_2)^+$. The counterions $BF_2Cl_2^-$, BF_3Cl^-, and BF_4^- were identified by resonances at δ −106, −128, and −149, respectively.[15] The relative amounts of the anions remain constant up to 30 °C but the overall intensity relative to the carbene increases in accord with successive replacement of F^- by Cl^- on the carbene. The initial formation of the CF_2 complex followed by successive replacement of F^- by Cl^- strongly supports the proposed exchange mechanism shown in eq 9–11.

The phosphine-substituted complex $CpFe(CO)(PPh_3)(CF_3)$ does not form the trihalomethyl compound $CpFe(CO)(PPh_3)(CCl_3)$ upon reaction with BCl_3 in analogy to the dicarbonyl (eq 6); instead, the phosphine stabilizes the carbene complexes that are intermediates in halogen exchange. At low temperature $CpFe(CO)(PPh_3)(CF_2)^+$ is observed. This is the intermediate formed in the first step of halogen exchange (eq 8). Upon increasing the temperature Cl^- is sequentially substituted for F^-, until $CpFe(CO)(PPh_3)(CCl_2)^+$ is the dominant species. Substitution of PPh_3 for a carbonyl ligand stabilizes carbene complexes by donating more electron density to the metal center.[16,17] For example, the phosphine-substituted complexes $Cp(CO)(PPh_3)Fe{=}CHR^+$ can be observed spectroscopically at −78 °C whereas the dicarbonyl complexes $Cp(CO)_2Fe{=}CHR^+$ are unstable at this temperature.[18] In the present case, substitution of PPh_3 for CO stabilizes the cationic dihalocarbene complexes $CpFe(CO)(PPh_3)(CF_xCl_{2-x})^+$, over the trihalomethyl complexes $CpFe(CO)(PPh_3)(CF_xCl_{3-x})$. Presumably, the trihalomethyl complexes $CpFe(CO)(PPh_3)(CF_xCl_{3-x})$ are intermediates in this exchange (eq 11).

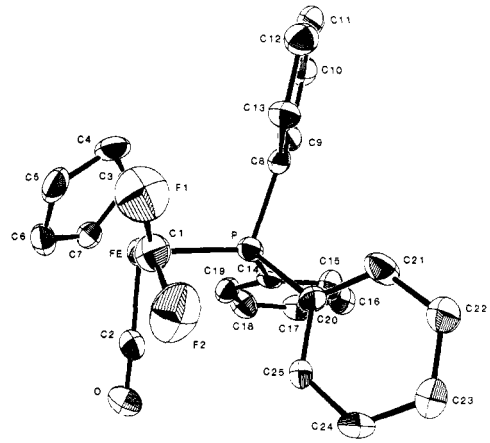

Figure 3. ORTEP diagram of $CpFe(CO)(PPh_3)(CF_2)^+$ with 50% probability ellipsoids, showing the numbering scheme. The hydrogen atoms have been omitted for clarity.

Table IV. Selected Bond Lengths (Å), Angles (deg), and Torsional Angles (deg) for $[CpFe(CO)(PPh_3)(CF_2)][BF_4]$[a]

Bond Lengths			
Fe–P	2.243 (3)	C(1)–F(1)	1.334 (10)
Fe–C(1)	1.724 (9)	C(1)–F(2)	1.334 (10)
Fe–C(2)	1.798 (10)	O–C(2)	1.113 (9)
Fe–C(3)	2.121 (8)	C(3)–C(4)	1.412 (12)
Fe–C(4)	2.108 (8)	C(4)–C(5)	1.420 (12)
Fe–C(5)	2.084 (8)	C(5)–C(6)	1.407 (12)
Fe–C(6)	2.097 (9)	C(6)–C(7)	1.417 (12)
Fe–C(7)	2.116 (8)	C(7)–C(3)	1.406 (11)
P–C(8)	1.828 (8)	B–F(3)	1.357 (13)
P–C(14)	1.822 (8)	B–F(4)	1.377 (13)
P–C(20)	1.806 (8)	B–F(5)	1.340 (13)
		B–F(6)	1.362 (13)

Bond Angles			
P–Fe–C(1)	92.4 (3)	Fe–C(2)–O	177.6 (8)
P–Fe–C(2)	95.5 (3)	C(3)–C(4)–C(5)	106.0 (8)
C(1)–Fe–C(2)	93.6 (4)	C(4)–C(5)–C(6)	109.6 (8)
Fe–P–C(8)	109.3 (3)	C(5)–C(6)–C(7)	107.1 (8)
Fe–P–C(14)	118.8 (3)	C(6)–C(7)–C(3)	107.9 (8)
Fe–P–C(20)	115.5 (3)	C(7)–C(3)–C(4)	109.4 (8)
C(8)–P–C(14)	103.7 (4)	Fe(3)–B–F(4)	107.7 (10)
C(8)–P–C(20)	107.2 (4)	F(3)–B–F(5)	111.7 (11)
C(14)–P–C(20)	101.1 (4)	F(3)–B–F(6)	109.3 (10)
Fe–C(1)–F(1)	130.3 (7)	F(4)–B–F(5)	109.2 (10)
Fe–C(1)–F(2)	131.3 (8)	F(4)–B–F(6)	106.8 (11)
F(1)–C(1)–F(2)	98.3 (7)	F(5)–B–F(6)	112.0 (11)

Torsional Angles			
C(2)–Fe–C(1)–F(2)	18 (1)[b]	P–Fe–C(1)–F(2)	−78 (1)

[a] Numbers in parentheses are estimated standard deviations in the least significant digits. See Figure 3 for numbering scheme. [b] Esd's for torsional angles are not available from the computing package used. The values given are estimated by considering the esd's of the other angles between the atoms involved in the torsional angle.

Structures. Both complexes 1 and 2 consist of discrete anions and cations with no unusually close interion distances. ORTEP diagrams showing the numbering systems are given in Figures 3 and 4. Bond distances, angles, and torsional angles are summarized in Tables IV and V.

The carbene moiety in $[CpFe(CO)_2(CCl_2)][BCl_4]$ adopts an orientation in which the plane described by the carbene bisects C(6)–Fe–C(7). The orientation of the Cp ring, with Cl(1) bisecting the C(2)–C(3) bond minimizes steric interaction between Cl(1) and the ring. The nonbonded distances Cl(1)–H(2) and Cl(1)–H(3) are approximately 3.1

(15) Hartman, J. S.; Schrobilgen, G. J. *Inorg. Chem.* **1972**, *11*, 940–951.
(16) Riley, P. E.; Capshew, C. E.; Pettit, R.; Davis, R. E. *Inorg. Chem.* **1978**, *17*, 408–414.
(17) Brookhart, M.; Tucker, J. R.; Flood, T. C.; Jensen, J. *J. Am. Chem. Soc.* **1980**, *102*, 1203–1205.
(18) Brookhart, M.; Tucker, J. R.; Husk, G. R. *J. Am. Chem. Soc.* **1983**, *105*, 258–264.

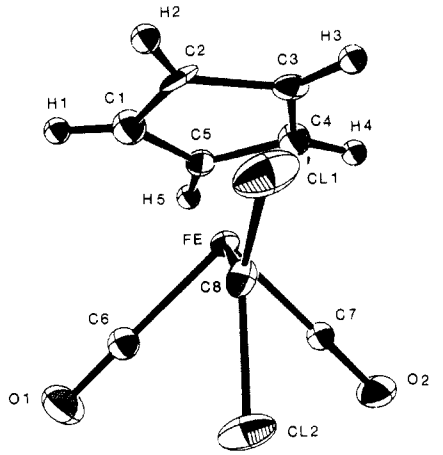

Figure 4. ORTEP diagram of $CpFe(CO)_2(CCl_2)^+$ with 50% probability ellipsoids, showing the numbering scheme.

Table V. Selected Bond Lengths (Å), Angles (deg), and Torsional Angles (deg) for $[CpFe(CO)_2(CCl_2)][BCl_4]$[a]

	Bond Lengths		
Fe–C(1)	2.059 (12)	C(6)–O(1)	1.132 (13)
Fe–C(2)	2.087 (10)	C(7)–O(2)	1.122 (12)
Fe–C(3)	2.103 (11)	C(1)–C(2)	1.368 (16)
Fe–C(4)	2.114 (11)	C(2)–C(3)	1.428 (15)
Fe–C(5)	2.078 (11)	C(3)–C(4)	1.397 (16)
Fe–C(6)	1.796 (12)	C(4)–C(5)	1.386 (16)
Fe–C(7)	1.805 (10)	C(5)–C(1)	1.407 (15)
Fe–C(8)	1.808 (12)	B–Cl(3)	1.876 (14)
Cl(1)–C(8)	1.694 (12)	B–Cl(4)	1.840 (12)
Cl(2)–C(8)	1.731 (11)	B–Cl(5)	1.826 (13)
		B–Cl(6)	1.845 (12)
	Bond Angles		
Fe–C(6)–O(1)	177.5 (10)	C(4)–C(5)–C(1)	107.1 (11)
Fe–C(7)–O(2)	178.9 (12)	C(5)–C(1)–C(2)	109.8 (11)
Fe–C(8)–Cl(5)	128.3 (7)	Cl(3)–B–Cl(4)	109.7 (7)
Fe–C(8)–Cl(2)	123.2 (7)	Cl(3)–B–Cl(5)	108.9 (6)
Cl(1)–C(8)–Cl(2)	108.5 (7)	Cl(3)–B–Cl(6)	108.5 (6)
C(6)–Fe–C(7)	90.6 (5)	Cl(4)–B–Cl(5)	110.5 (7)
C(1)–C(2)–C(3)	106.9 (10)	Cl(4)–B–Cl(6)	109.2 (6)
C(2)–C(3)–C(4)	107.6 (11)	Cl(5)–B–Cl(6)	110.0 (7)
C(3)–C(4)–C(5)	108.6 (10)		
	Torsional Angles		
C(2)–Fe–C(8)–Cl(1)	19 (2)[b]	C(6)–Fe–C(8)–Cl(2)	−47 (2)
C(3)–Fe–C(8)–Cl(1)	−21 (2)	C(7)–Fe–C(8)–Cl(2)	44 (2)

[a] Numbers in parentheses are estimated standard deviations in the least significant digits. See Figure 4 for numbering scheme. [b] Eds's for torsional angles are not available from the computing package used. The values given are estimated by considering the esd's of the other angles between the atoms involved in the torsional angle.

Å. The Fe–C(8) distance, 1.808 Å, is approximately equal to the Fe–C carbonyl distances, indicating that the carbene group behaves as a good π-acceptor. A similar Fe–C carbene distance of 1.83 Å is found for $Fe(TPP)(CCl_2)(H_2O)$.[19] The bond lengths and angles around the CCl_2 group agree closely with those found for Roper's complex $IrCl_3(CCl_2)(PPh_3)_2$, where C–Cl is 1.72 Å and the angle Cl–C–Cl is 107.5°.[6]

The carbene moiety in compound **1** is nearly coplanar with the carbonyl but is tilted 18.0° toward the Fe–P bond. The F(1)–C(1)–F(2) bond angle of 98.3° is small compared to the F–C–F angle of 110.1° in 1,1-difluoroethane but large compared to Roper's difluorocarbene complex $[Ru(CF_2)(CO)_2(PPh_3)_2]$, where the F–C–F angle is 88.7°.[7,20] The very short Fe–C(1) distance of 1.724 Å in $CpFe(CO)(PPh_3)(CF_2)^+$ indicates that the CF_2 group is a potent π-acceptor, owing to the high electronegativity of the fluorines. Similarly, the replacement of one phenyl group by fluorine in $CpMn(CO)_2(CPh_2)$ decreases the Mn–C(carbene) distance from 1.885 (2) to 1.830 (5) Å.[21,22] The short Mn–C(carbene) and long C–F bonds in $CpMn(CO)_2(CFPh)$ are rationalized according to an ionic resonance form in which F^- is dissociated.[22] The short M–C(carbene) bonds in **1** and in $CpMn(CO)_2(CFPh)$ are consistent with Bent's rule, which states that hybrid orbitals directed toward electronegative elements will be depleted in s character.[25,26] An electronegative element bonded to a central atom will cause a shortening of the other bonds to that atom. On this basis, the Fe–C(carbene) bond in **1** should be short. Bent's rule also predicts that the angle in a molecule X–A–X should decrease as the electronegativity of X increases.[25,26] For example, the angle of the free CF_2 fragment in the ground state has been determined experimentally and by theoretical calculations to be 105°.[27–30] Therefore, it is not surprising that the F–C–F angle is **1** in smaller than a normal sp^2 bond angle. However, it is not clear why the F–C–F angles vary so greatly between **1**, $Ru(CF_2)(CO)_2(PPh_3)_2$, and 1,1-difluoroethane.[7,20]

The orientation of the carbene ligands in compounds **1** and **2** agree with the conformations predicted by MO theory.[9–11] The dichlorocarbene moiety in compound **2** is within 3° of the expected vertical conformation, in contrast to $[Cp(\eta^1\text{-CHT})Fe(CO)_2][PF_6]$, CHT = C_7H_6 or $C_{11}H_{18}$, in which steric factors force the carbene into the electronically less favorable horizontal conformation.[31] The X-ray structure of $CpMn(CO)_2[C(C_6H_5)_2]$ shows the predicted vertical conformation.[21,23] In Selegue's ruthenium dimer $[Ru_2(\mu\text{-}C_{10}H_{12})(PPh_3)_4(Cp)_2][PF_6]$, one ruthenium atom is bonded to a carbene moiety in the vertical conformation, and the other has a vinylidene linkage in the horizontal conformation, as predicted by Hoffman and co-workers.[9,32]

In compound **1**, the carbene is rotated toward CO, a better π-acceptor than PPh_3. Similar orientations have been observed crystallographically for $CpCr(CO)(NO)[C(C_6H_5)_2]$, and $[CpRe(NO)(PPh_3)(CHC_6H_5)][PF_6]$ where the carbene is in line with the better π-acceptor NO^+.[21,33]

Conformation of $[CpFe(CO)(PPh_3)(CF_2)][BF_4]$ in Solution. The ^{19}F NMR spectra of compound **2** in CD_2Cl_2 show a single sharp peak at δ +164 due to the difluorocarbene from room temperature to −80 °C. Since no conformation exists in which both fluorines are equivalent, rotation around the Fe–C(1) bond must be rapid throughout this temperature range.

Although **1** adopts the predicted conformation in the

(19) Mansuy, D.; Lange, M.; Chottard, J. C.; Bartoli, J. F.; Chevrier, B.; Weiss, R. *Angew. Chem., Int. Ed. Engl.* **1978**, *17*, 781–782.
(20) Chauffroureaux, J. C. *J. Phys.* **1967**, *28*, 344–348.
(21) Herrmann, W. A.; Hubbard, J. L.; Bernal, I.; Korp, J. D.; Haymore, B. L.; Hillhouse, G. L. *Inorg. Chem.* **1984**, *23*, 2978–2983.
(22) Fischer, E. O.; Kleine, W.; Schambeck, W.; Schubert, U. *Z. Naturforsch., B: Anorg. Chem.* **1981**, *36B*, 1575–1580.
(23) Herrmann, W. A. *Chem. Ber.* **1975**, *108*, 486–499.
(24) Friedrich, P.; Besl, G.; Fischer, E. O.; Huttner, G. *J. Organomet. Chem.* **1977**, *139*, C68–C72.
(25) Bent, H. A. *Chem. Rev.* **1961**, *61*, 275–311.
(26) Bent, H. A. *J. Chem. Educ.* **1960**, *37*, 616–624.
(27) Harrison, J. R. *J. Am. Chem. Soc.* **1971**, *93*, 4112–4119.
(28) Mathews, C. W. *Can. J. Phys.* **1967**, *45*, 2355–2374.
(29) Powell, F. X.; Lide, F. R., Jr. *J. Chem. Phys.* **1966**, *45*, 1067–1068.
(30) Mathews, C. W. *J. Chem. Phys.* **1966**, *45*, 1068.
(31) Riley, P. E.; Davis, R. E.; Allison, N. T.; Jones, W. M. *Inorg. Chem.* **1982**, *21*, 1321–1328.
(32) Selegue, J. P. *J. Am. Chem. Soc.* **1983**, *105*, 5921–5923.
(33) Kiel, W. A.; Lin, G. L.; Constable, A. G.; McCormick, F. B.; Strouse, C. E.; Eisenstein, O.; Gladysz, J. A. *J. Am. Chem. Soc.* **1982**, *104*, 4865–4878.

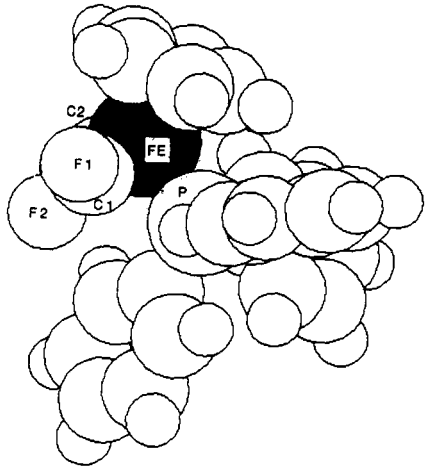

Figure 5. Space-filling diagram of $CpFe(CO)(PPh_3)(CF_2)^+$.

solid state, variable-temperature ^{19}F NMR data in solution indicate that the barrier to rotation around the Fe–C(1) bond must be quite low. Free rotation also occurs around the Mn–carbene bond in $CpMn(CO)_2[C(CH_3)_2]$ down to at least −55 °C, but it adopts the vertical orientation in the solid state.[34,35] In contrast, $CpRe(NO)(PPh_3)(CHC_6H_5)^+$ does not rotate around the Re–carbene bond from −78 to +20 °C at which point it switches to a new geometric isomer.[33] The Cr–carbene bond in $CpCr(NO)(CO)[C(C_6H_5)_2]$ shows hindered rotation at room temperature, whereas the Mn–carbene bond in $CpMn(CO)_2[C(C_6H_5)_2]$ rotates freely.[21,23] In general, the barrier for M–carbene bond rotation appears to be larger for the substituted complexes than for the dicarbonyls, except in the case of **1**. In addition, the carbene ligands in $CpCr(NO)(CO)[C(C_6H_5)_2]$ and $CpRe(NO)(PPh_3)[CH(C_6H_5)]^+$ are twisted by only 2–4° from alignment with NO,[21,33] whereas the CF_2 ligand in compound **1** is twisted 18° from alignment with CO. The difference may stem from the orbital splitting and reorientation that occurs when CO is replaced by nitrosyl or a phosphine. The difference in π-accepting ability is larger between CO and NO than between CO and PH_3. Because of this difference the splitting of the metal d orbitals is smaller in the phosphine case, so the orientational effects are less pronounced.[10]

Steric effects also may play a role in the orientation of the CF_2 fragment. For $CpM(CO)(PPh_3)$(carbene) complexes steric crowding of the carbene by a phenyl group on PPh_3 causes stereoselective addition of nucleophiles to the carbene.[36,37] The space-filling diagram in Figure 5 shows the interaction between the carbene and PPh_3.[38] The closest contact between the CF_2 moiety and the phenyl rings is 3.04 Å, between F(2) and the hydrogen atom on C(25). This model suggests that steric interaction with a phenyl ring contributes to the alignment of the carbene with CO.

Conclusions

Substitution of triphenylphosphine for carbonyl alters both the reactivity and solid-state conformation of $CpFe(CO)(PPh_3)(CF_2)^+$. Increased electron density on the metal center stabilizes the carbene over the trihalomethyl form, which allows observation of the carbene intermediates in halogen exchange with BCl_3. The carbene reorients from a vertical conformation in $[CpFe(CO)_2(CCl_2)][BCl_4]$ to near coplanarity with CO in $[CpFe(CO)(PPh_3)(CF_2)][BF_4]$ as predicted by MO calculations. However, the conformational effect is not as large as for NO^+ substitution, due to decreased orbital splitting. Since the orbital requirements are not overpowering, steric factors also appear to affect the carbene orientation.

Acknowledgment. We appreciate the support of this research by the National Science Foundation. A.M.C. thanks Dr. P. N. Swepston and J. A. Hriljac for their help with the X-ray crystallography.

Supplementary Material Available: Tables of anisotropic thermal parameters, calculated hydrogen atom positions, and additional bond lengths and angles and a listing of observed and calculated structure factor amplitudes for **1** and **2** (47 pages). Ordering information is given on any current masthead page.

(34) Fischer, E. O.; Clough, R. L.; Besl, G.; Kreissl, F. R. *Angew. Chem., Int. Ed. Engl.* **1976**, *15*, 543–544.

(35) Friedrick, P.; Besl, G.; Fischer, E. O.; Huttner, G. *J. Organomet. Chem.* **1977**, *139*, C68–C72.

(36) Davies, S. G.; Seeman, J. I. *Tetrahedron Lett.* **1984**, *25*, 1845–1848.

(37) Baird, G. J.; Davies, S. G.; Maberly, T. R. *Organometallics* **1984**, *3*, 1765–1767.

(38) Space-filling diagram generated by CHEMGRAF, K. Davies, Oxford, Jan 1983–1984, using crystallographically determined atomic coordinates.